Letters

Interoperability Study of Electric Vehicle Wireless Charging System Based on LCC-S Compensation Using Two Decoupled Unipolar Transmitting Coils

Bo Cheng, Jingchen Song, Zhaoyong Mao, Rongbin Liu, Ronghuan Xie, Xingkui Mao, and Yiming Zhang, *Senior Member, IEEE*

***Abstract*—This letter presents a novel wireless power transfer (WPT) system for electric vehicles (EVs) that addresses interoperability issues among different coil types. The proposed solution utilizes two mutually decoupled unipolar transmitting coils with an inductor-capacitor-capacitor series compensation topology. By regulating the switching sequence of a dual-phase inverter, the current directions in the transmitting coils can be reconfigured to ensure compatibility with both unipolar and bipolar receiving coils. Additionally, a mode-switching strategy based on the proposed coil design enhances the robustness of the system against misalignment within its operational range. Experimental results validate the interoperability for unipolar and bipolar coils and demonstrate misalignment tolerance performance along specific directions.**

***Index Terms*—Decoupled transmitting coils, inductor-capacitor-capacitor series (LCC-S), interoperability, wireless power transfer (WPT).**

I. Introduction

With the rapid development of electric vehicles (EVs), wireless power transmission (WPT) has gained favor in academia and industry due to its reliability, safety, convenience, and automation in power transmission [1], [2], [3]. In a typical EV WPT system, the ground components and on-board components have different models and versions, achieving energy interconnection through information interaction and control [4], [5]. The interoperability of wireless charging systems can be categorized into three key categories: interoperability of communication systems, interoperability of compensation networks, and interoperability of magnetic couplers [6], [7].

To achieve coil interoperability, EV WPT systems can incorporate various coil types, such as unipolar, bipolar, and quadrupolar coils [8], [9], [10]. Among them, unipolar coils and bipolar coils are the most used coil configurations. However, power transmission is hindered by the mutual decoupling between different coils. Solving coil interoperability is essential for ensuring compatibility across manufacturers and promoting the widespread commercialization of WPT technology Achieving coil interoperability is crucial for the widespread commercialization of WPT technology [11], [12].

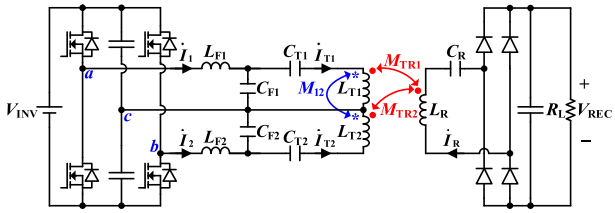

Fig. 1. Proposed topology.

Extensive research has been conducted globally to address coil interoperability. Technical advancements have improved universal coil interoperability; for instance, an adaptive position adjustment scheme was proposed in [13] to achieve interoperability between unipolar and bipolar coils, but it requires continuous searching for the maximum dc input current to locate the optimal transmitter position. Other approaches include stacked unipolar and bipolar coils with switched main transmission coils [14], [15], and a nonoverlapping scheme using three decoupled unipolar coils that alters current direction to solve interoperability [16]. While these methods avoid specific installation requirements, they often involve large coil sizes. A vector synthesis strategy with multiple decoupled coils was proposed in [17] to effectively address multicoil interoperability, but it demands complex design and control strategies. Existing solutions face challenges such as high production costs and practical implementation difficulties.

To be compatible with both unipolar and bipolar coils, this letter proposes an LCC-S compensated WPT system for EVs based on two unipolar coils. The two transmitting coils are mutually decoupled. By adjusting the conduction sequence of the system, the transmitting current directions are reconfigured to achieve interoperability. Additionally, a mode-switching control strategy is introduced to mitigate efficiency reduction under

Received 15 June 2025; revised 23 July 2025, 4 September 2025, and 11 October 2025; accepted 24 October 2025. Date of publication 28 October 2025; date of current version 19 January 2026. This work was supported by the National Natural Science Foundation of China under Grant 52577187. *(Corresponding authors: Ronghuan Xie; Xingkui Mao; Yiming Zhang.)*

Bo Cheng, Jingchen Song, and Zhaoyong Mao are with Unmanned System Research Institute, Northwestern Polytechnical University, Xi'an 710072, China (e-mail: chengbo@nwpu.edu.cn; huaqing@mail.nwpu.edu.cn; maozhaoyong@nwpu.edu.cn).

Rongbin Liu, Ronghuan Xie, Xingkui Mao, and Yiming Zhang are with the School of Electrical Engineering and Automation, Fuzhou University, Fuzhou 350108, China (e-mail: 220127070@fzu.edu.cn; 2500110011@fzu.edu.cn; mxk782@fzu.edu.cn; zym@fzu.edu.cn).

Color versions of one or more figures in this article are available at https://doi.org/10.1109/TPEL.2025.3626344.

Digital Object Identifier 10.1109/TPEL.2025.3626344

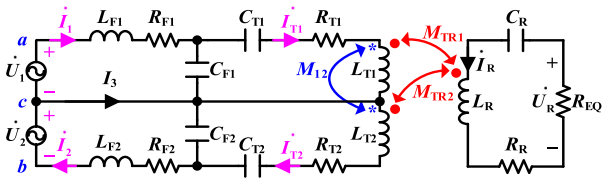

Fig. 2. Equivalent circuit of Mode I.

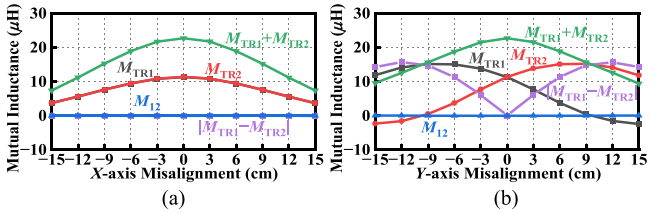

Fig. 3. Mutual inductance variation with misalignment in Mode I. (a) Along X-axis. (b) Along Y-axis.

misalignment conditions. The voltage threshold is determined from measured mutual inductance; when the output voltage falls to this threshold, the system adjusts the current direction to maintain positive coupling, thereby enhancing transmission efficiency.

II. Topology and Modeling

The topology of the proposed system is shown in Fig. 1. V_{INV} and V_{REC} denote the dc voltages of the inverter and rectifier, respectively. L_{F1} and L_{F2} are series compensation inductors, with currents $\dot{I}_1$ and $\dot{I}_2$ flowing through them. C_{F1} and C_{F2} are parallel compensation capacitors. L_{T1} and L_{T2} represent the self-inductances of the two transmitting coils, compensated in series by C_{T1} and C_{T2}. The corresponding coil currents are $\dot{I}_{\mathrm{T1}}$ and $\dot{I}_{\mathrm{T2}}$. On the receiving side, L_{R} and C_{R} are the self-inductance and compensation capacitor of the receiving coil, with current $\dot{I}_{\mathrm{R}}$. M_{TR1} and M_{TR2} are the mutual inductances between the transmitting coils and the receiving coil, while M_{12} is the mutual inductance between L_{T1} and L_{T2}. R_{L} is the load resistance.

The system operates at the resonant angular frequency ω

$$\omega = \frac{1}{\sqrt{L_{\mathrm{R}}C_{\mathrm{R}}}} = \frac{1}{\sqrt{L_{\mathrm{F1}}C_{\mathrm{F1}}}} = \frac{1}{\sqrt{L_{\mathrm{F2}}C_{\mathrm{F2}}}} = \frac{1}{\sqrt{L_{\mathrm{T1}}\left(C_{\mathrm{F1}}//C_{\mathrm{T1}}\right)}} = \frac{1}{\sqrt{L_{\mathrm{T2}}\left(C_{\mathrm{F2}}//C_{\mathrm{T2}}\right)}}. \tag{1}$$

A. Mode I: Unipolar Coil As Receiving Coil

When the receiving coil is unipolar, the system operates in Mode I. The equivalent circuit is shown in Fig. 2. $\dot{U}_1$ and $\dot{U}_2$ represent the fundamental components of ac input voltages in the inverter, while $\dot{U}_R$ denotes the ac output voltage of the rectifier. R_{EQ} is the equivalent ac load resistance. $R_{\mathrm{F1}}, R_{\mathrm{F2}}, R_{\mathrm{T1}}, R_{\mathrm{T2}}$, and R_{R} are the equivalent series resistances (ESRs). These quantities can be expressed as

$$U_1 = U_2 = \frac{\sqrt{2}}{\pi}V_{\mathrm{INV}}, U_{\mathrm{R}} = \frac{2\sqrt{2}}{\pi}V_{\mathrm{REC}} \tag{2}$$

$$R_{\mathrm{EQ}} = \frac{8}{\pi^2}R_{\mathrm{L}}, R_{\mathrm{X}} = \frac{\omega L_{\mathrm{X}}}{Q} \tag{3}$$

where L_{X} and R_{X} represent the inductance and ESR of any branch, respectively, and Q represents the quality factor.

When the system operates at its resonant frequency, based on Kirchhoff's Voltage Law (KVL), one can get

$$\begin{cases} \dot{U}_1 = R_{\mathrm{F1}}\dot{I}_1 + j\omega L_{\mathrm{F1}}\dot{I}_{\mathrm{T1}} \\ \dot{U}_2 = R_{\mathrm{F2}}\dot{I}_2 + j\omega L_{\mathrm{F2}}\dot{I}_{\mathrm{T2}} \\ -j\omega L_{\mathrm{F1}}\dot{I}_1 = R_{\mathrm{T1}}\dot{I}_{\mathrm{T1}} + j\omega M_{\mathrm{TR1}}\dot{I}_{\mathrm{R}} \\ -j\omega L_{\mathrm{F2}}\dot{I}_2 = R_{\mathrm{T2}}\dot{I}_{\mathrm{T2}} + j\omega M_{\mathrm{TR2}}\dot{I}_{\mathrm{R}} \\ \dot{I}_{\mathrm{R}}\left(R_{\mathrm{EQ}} + R_{\mathrm{R}}\right) + j\omega M_{\mathrm{TR1}}\dot{I}_{\mathrm{T1}} + j\omega M_{\mathrm{TR2}}\dot{I}_{\mathrm{T2}} = 0. \end{cases} \tag{4}$$

$\dot{I}_R$ can be solved as

$$\dot{I}_{\mathrm{R}} = \frac{\sum_{i=1}^{2}\frac{\omega^2 M_{\mathrm{TRi}}L_{\mathrm{Fi}}\dot{U}_{\mathrm{i}}}{\omega^2 L_{\mathrm{Fi}}^2 + R_{\mathrm{Fi}}R_{\mathrm{Ti}}}}{R_{\mathrm{EQ}} + R_{\mathrm{R}} + \sum_{i=1}^{2}\frac{\omega^2 M_{\mathrm{TRi}}^2 R_{\mathrm{Fi}}}{\omega^2 L_{\mathrm{Fi}}^2 + R_{\mathrm{Fi}}R_{\mathrm{Ti}}}}. \tag{5}$$

Therefore, the output voltage and output power can be expressed as

$$V_{\mathrm{REC}} = \frac{2\sqrt{2}\pi R_{\mathrm{L}}\sum_{i=1}^{2}\frac{\omega^2 M_{\mathrm{TRi}}L_{\mathrm{Fi}}U_{\mathrm{i}}}{\omega^2 L_{\mathrm{Fi}}^2 + R_{\mathrm{Fi}}R_{\mathrm{Ti}}}}{8R_{\mathrm{L}} + \pi^2 R_{\mathrm{R}} + \pi^2\sum_{i=1}^{2}\frac{\omega^2 M_{\mathrm{TRi}}^2 R_{\mathrm{Fi}}}{\omega^2 L_{\mathrm{Fi}}^2 + R_{\mathrm{Fi}}R_{\mathrm{Ti}}}} \tag{6}$$

$$P_{\mathrm{OUT}} = \frac{V_{\mathrm{REC}}^2}{R_{\mathrm{L}}} = \frac{8\pi^2 R_{\mathrm{L}}\left(\sum_{i=1}^{2}\frac{\omega^2 M_{\mathrm{TRi}}L_{\mathrm{Fi}}U_{\mathrm{i}}}{\omega^2 L_{\mathrm{Fi}}^2 + R_{\mathrm{Fi}}R_{\mathrm{Ti}}}\right)^2}{\left(8R_{\mathrm{L}} + \pi^2 R_{\mathrm{R}} + \pi^2\sum_{i=1}^{2}\frac{\omega^2 M_{\mathrm{TRi}}^2 R_{\mathrm{Fi}}}{\omega^2 L_{\mathrm{Fi}}^2 + R_{\mathrm{Fi}}R_{\mathrm{Ti}}}\right)^2}. \tag{7}$$

Given that Q typically ranges between 300 and 400, indicating that ESRs are far smaller than the inductive impedance and can be neglected. When the proposed system is fully symmetric, it satisfies $U_1 = U_2 = U, L_{\mathrm{F1}} = L_{\mathrm{F2}} = L_{\mathrm{F}}$, and $L_{\mathrm{T1}} = L_{\mathrm{T2}} = L_{\mathrm{T}}$. Under these conditions, (5), (6), and (7) can be simplified as

$$I_{\mathrm{R}} = \frac{\left(M_{\mathrm{TR1}} + M_{\mathrm{TR2}}\right)U}{R_{\mathrm{EQ}}L_{\mathrm{F}}} \tag{8}$$

$$V_{\mathrm{REC}} = \frac{\left(M_{\mathrm{TR1}} + M_{\mathrm{TR2}}\right)V_{\mathrm{INV}}}{2L_{\mathrm{F}}} \tag{9}$$

$$P_{\mathrm{OUT}} = \frac{\left(M_{\mathrm{TR1}} + M_{\mathrm{TR2}}\right)^2 V_{\mathrm{INV}}^2}{4R_{\mathrm{L}}L_{\mathrm{F}}^2}. \tag{10}$$

As shown in (9), the output voltage is proportional to the sum of the mutual inductances. When misalignment occurs, the mutual inductances vary accordingly. Within the *XY*-plane from –150 to 150 mm, the sum of the mutual inductances remains consistently greater than zero, as shown in Fig. 3. By adjusting the conduction sequence of switches, L_{T1} and L_{T2} produce magnetic fields in the same direction, enabling energy transfer to the unipolar receiving coil. Furthermore, the mutual inductance between the two transmitting coils remains close to zero, indicating strong decoupling.

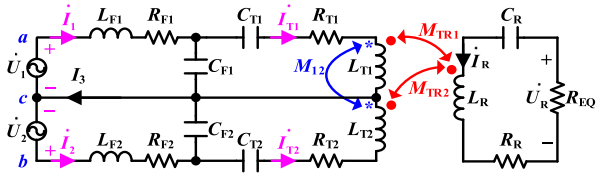

Fig. 4. Equivalent circuit of Mode II.

The calculation of system efficiency must account for the ESRs, and is therefore derived as

$$Eff = \frac{P_{\mathrm{OUT}}}{P_{\mathrm{OUT}} + \sum I_{\mathrm{X}}^2 R_{\mathrm{X}}} \tag{11}$$

where I_{X} represent the current of any branch.

Combining the above equations yields

$$Eff = \frac{1}{1+\frac{\omega\pi^2}{8R_{\mathrm{L}}Q}\left[L_{\mathrm{R}}+\frac{\left(M_{\mathrm{TR1}}^2+M_{\mathrm{TR2}}^2\right)^2}{L_{\mathrm{F}}}\right]+\frac{8R_{\mathrm{L}}L_{\mathrm{T}}}{\omega\pi^2 Q(M_{\mathrm{TR1}}+M_{\mathrm{TR2}})^2}}. \tag{12}$$

Misalignment along the *Y*-axis leads to a sharp reduction in transmission efficiency, because one of the mutual inductances turns negative, reducing their combined value. As indicated by the third term in the denominator of (12), converting this negative contribution to positive will improve system efficiency. By introducing voltage feedback to monitor the output voltage, the system can automatically switch from Mode I to Mode II, effectively increasing transmission efficiency.

B. Mode II: Bipolar Coil As Receiving Coil

When the receiving coil is bipolar, the system operates in Mode II. The equivalent circuit is shown in Fig. 4. Based on KVL, one can get

$$\begin{cases} \dot{U}_1 = R_{\mathrm{F1}}\dot{I}_1 + j\omega L_{\mathrm{F1}}\dot{I}_{\mathrm{T1}} \\ \dot{U}_2 = R_{\mathrm{F2}}\dot{I}_2 + j\omega L_{\mathrm{F2}}\dot{I}_{\mathrm{T2}} \\ -j\omega L_{\mathrm{F1}}\dot{I}_1 = R_{\mathrm{T1}}\dot{I}_{\mathrm{T1}} + j\omega M_{\mathrm{TR1}}\dot{I}_{\mathrm{R}} \\ -j\omega L_{\mathrm{F2}}\dot{I}_2 = R_{\mathrm{T2}}\dot{I}_{\mathrm{T2}} - j\omega M_{\mathrm{TR2}}\dot{I}_{\mathrm{R}} \\ \dot{I}_{\mathrm{R}}\left(R_{\mathrm{EQ}}+R_{\mathrm{R}}\right) + j\omega M_{\mathrm{TR1}}\dot{I}_{\mathrm{T1}} - j\omega M_{\mathrm{TR2}}\dot{I}_{\mathrm{T2}} = 0 \end{cases}. \tag{13}$$

In this mode, $\dot{U}_1 = -\dot{U}_2$. $\dot{I}_R$ can be solved as

$$\dot{I}_{\mathrm{R}} = \frac{\sum_{i=1}^{2}\frac{(-1)^i\omega^2 M_{\mathrm{TRi}}L_{\mathrm{Fi}}\dot{U}_{\mathrm{i}}}{\omega^2 L_{\mathrm{Fi}}^2+R_{\mathrm{Fi}}R_{\mathrm{Ti}}}}{R_{\mathrm{EQ}}+R_{\mathrm{R}}+\sum_{i=1}^{2}\frac{\omega^2 M_{\mathrm{TRi}}^2 R_{\mathrm{Fi}}}{\omega^2 L_{\mathrm{Fi}}^2+R_{\mathrm{Fi}}R_{\mathrm{Ti}}}}}. \tag{14}$$

Therefore, the output voltage and output power can be expressed as

$$V_{\mathrm{REC}} = \frac{2\sqrt{2}\pi R_{\mathrm{L}}\sum_{i=1}^{2}\frac{\omega^2 M_{\mathrm{TRi}}L_{\mathrm{Fi}}U_{\mathrm{i}}}{\omega^2 L_{\mathrm{Fi}}^2+R_{\mathrm{Fi}}R_{\mathrm{Ti}}}}{8R_{\mathrm{L}}+\pi^2 R_{\mathrm{R}}+\pi^2\sum_{i=1}^{2}\frac{\omega^2 M_{\mathrm{TRi}}^2 R_{\mathrm{Fi}}}{\omega^2 L_{\mathrm{Fi}}^2+R_{\mathrm{Fi}}R_{\mathrm{Ti}}}}} \tag{15}$$

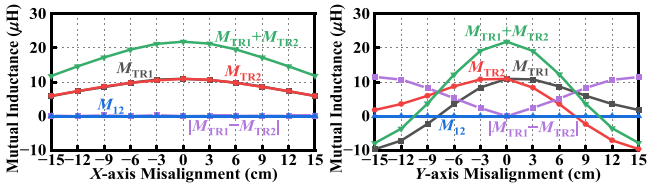

Fig. 5. Mutual inductance variation with misalignment in Mode II. (a) Along X-axis. (b) Along Y-axis.

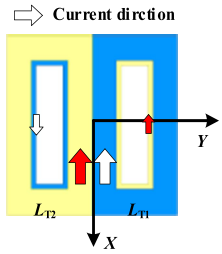

Fig. 6. Proposed two unipolar decoupling coils.

$$P_{\mathrm{OUT}} = \frac{V_{\mathrm{REC}}^2}{R_{\mathrm{L}}} = \frac{8\pi^2 R_{\mathrm{L}}\left(\sum_{i=1}^{2}\frac{\omega^2 M_{\mathrm{TRi}}L_{\mathrm{Fi}}U_{\mathrm{i}}}{\omega^2 L_{\mathrm{Fi}}^2+R_{\mathrm{Fi}}R_{\mathrm{Ti}}}\right)^2}{\left(8R_{\mathrm{L}}+\pi^2 R_{\mathrm{R}}+\pi^2\sum_{i=1}^{2}\frac{\omega^2 M_{\mathrm{TRi}}^2 R_{\mathrm{Fi}}}{\omega^2 L_{\mathrm{Fi}}^2+R_{\mathrm{Fi}}R_{\mathrm{Ti}}}\right)^2}. \tag{16}$$

When the proposed system is fully symmetric, (14), (15), and (16) can be further simplified as

$$I_{\mathrm{R}} = \frac{\left(M_{\mathrm{TR1}}+M_{\mathrm{TR2}}\right)U}{R_{\mathrm{EQ}}L_{\mathrm{F}}} \tag{17}$$

$$V_{\mathrm{REC}} = \frac{\left(M_{\mathrm{TR1}}+M_{\mathrm{TR2}}\right)V_{\mathrm{INV}}}{2L_{\mathrm{F}}} \tag{18}$$

$$P_{\mathrm{OUT}} = \frac{\left(M_{\mathrm{TR1}}+M_{\mathrm{TR2}}\right)^2 V_{\mathrm{INV}}^2}{4R_{\mathrm{L}}L_{\mathrm{F}}^2}. \tag{19}$$

As indicated in (18), the output voltage is proportional to the sum of the mutual inductances. These values vary with misalignment, as depicted in Fig. 5. By adjusting the conduction sequence of the inverter, L_{T1} and L_{T2} produce opposing magnetic fields, which enables efficient energy transfer to the bipolar receiving coil. The two transmitting coils in this mode are also decoupled.

The efficiency expression for Mode II is the same as for Mode I. As the misalignment along the *Y*-axis increases, the sum of the mutual inductances approaches zero, impeding power transfer. The control strategy similar to that in Mode I can be applied: converting the negative mutual inductance to positive enhances system efficiency. When the output voltage falls below a threshold, the system automatically switches from Mode II back to Mode I, thereby effectively improving transmission efficiency.

III. Magnetic Design

To achieve compatibility with both unipolar and bipolar receiving coils, the transmitting coil assembly comprises two independent unipolar coils, as shown in Fig. 6. Although multicoil configurations typically produce cross-coupling, the proposed

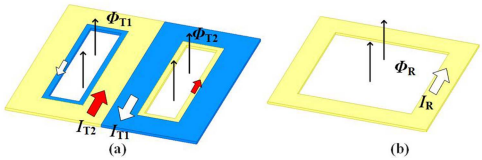

Fig. 7. Current direction of the coil in Mode I. (a) Proposed coil structure. (b) Unipolar coil.

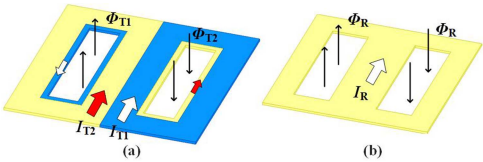

Fig. 8. Current direction of the coil in Mode II. (a) Proposed coil structure. (b) Bipolar coil.

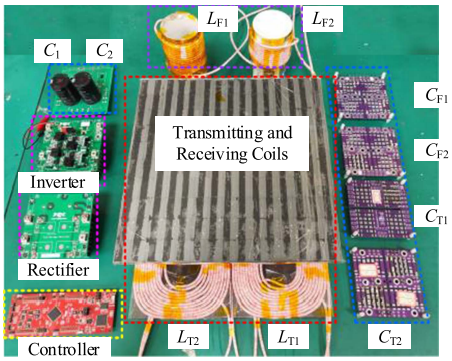

Fig. 9. Experimental prototype.

design employs decoupled coils positioned concentrically to mitigate interference. Specifically, the decoupling coil for L_{T1} cancels the magnetic flux generated by L_{T1} in L_{T2}, and vice versa, thereby effectively eliminating mutual interference. As shown in Figs. 3 and 5, the cross mutual inductance M_{12} remains close to zero across the XY-plane from –150 to 150 mm, demonstrating excellent decoupling performance throughout the entire operating range.

When a unipolar or bipolar receiving coil is used, the system operates in Mode I or Mode II, respectively. Figs. 7 and 8 illustrate the current directions in the proposed coil under both modes Here, Φ_{T1}, Φ_{T2}, and Φ_R represent the magnetic flux directions produced by the transmitting coils and the receiving coil. To achieve efficient energy transfer, both transmitting coils must remain positively coupled with the receiving coil.

When Y-axis misalignment exceeds ±90 mm, one transmitting coil becomes negatively coupled with the receiving coil, weakening the coupling and reducing energy transfer efficiency. As shown in (12), the higher sum of mutual inductances leads to improved transmission efficiency. To address this issue, this letter proposes a mode-switching control strategy. The output voltage decreases to a threshold as the misalignment increases. At this point, by adjusting the direction of the transmitting current, the system ensures that the transmitting coil and both types of receiving coils remain positively coupled across the misalignment range, thereby maintaining efficient energy transfer.

TABLE I
PARAMETERS OF EXPERIMENTAL PROTOTYPE

V_{INV}	200 V	f	85 kHz	R_L	10 Ω
L_{F1}	18.20 μH	C_{F1}	191.90 nF	C_1	470 nF
L_{F2}	18.65 μH	C_{F2}	190.50 nF	C_2	470 nF
L_{T1}	49.52 μH	C_{T1}	112.20 nF	–	–
L_{T2}	49.44 μH	C_{T2}	112.29 nF	–	–
L_R	113.02 μH	C_R	30.80 nF	–	–

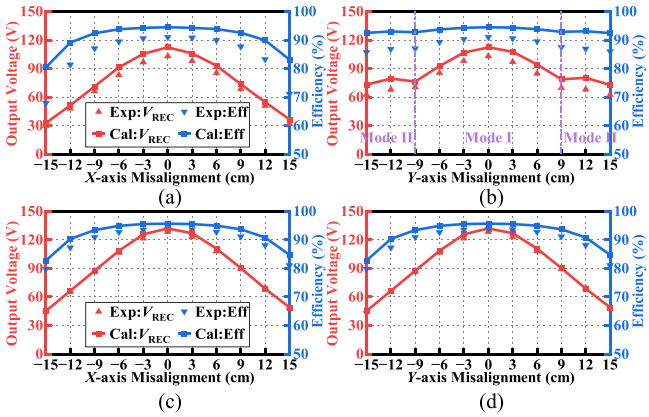

Fig. 10. Output voltage and efficiency in Mode I. (a) Proposed (X-axis). (b) Proposed (Y-axis). (c) Traditional (X-axis). (d) Traditional (Y-axis).

The voltage threshold is designed based on measured mutual inductance. Different magnetic couplers exhibit distinct trends in mutual inductance variation. A practical method involves measuring the curves of mutual inductance sum and difference. The misalignment position at which these two curves intersect is defined as the mode switching point. Due to the monotonic correlation between output voltage and misalignment, the output voltage at this point is used as the voltage threshold for mode switching.

IV. EXPERIMENTAL VALIDATION

An experimental prototype was constructed to validate the proposed system, as shown in Fig. 9. The experimental parameters are summarized in Table I. The transmitting and receiving coils both measure 300 mm × 300 mm, with a charging distance of 100 mm. Each transmitting coil has 10 turns, while the reverse winding consists of 2 turns.

Experimental results are presented in Figs. 10(a) and (b) and 11(a) and (b). The test range covers a plane from −150 to 150 mm in both the X-axis and Y-axis. The calculated results are closely aligned with the experimental ones, confirming the accuracy of the theoretical model. To further assess the performance of the proposed system, comparative experiments are carried out under identical conditions using traditional unipolar and bipolar coils with equivalent dimensions and number of turns. These results are provided in Figs. 10(c) and (d) and 11(c) and (d).

Under perfect alignment, both modes achieve comparable output power and efficiency exceeding 90%, matching

TABLE II
COMPARISONS WITH EXISTING SCHEMES.

Scheme	Power Density (W/cm3)	Efficiency range (>80%) (mm)	Coil Complexity	Control Complexity	Compatibility Coil Type	Decoupling Method
[12]	Unipolar Mode: 0.12	*X*-axis: [−200,200] *Y*-axis: [−240,240]	Medium (Decoupled Mutually Spliced DD Coil, 300×400 mm)	Medium (Dual-Channel Control)	Unipolar, Bipolar and Quadrupolar	Reverse Winding
	Bipolar Mode: 0.12	*X*-axis: [−160,160] *Y*-axis: [−120,120]				
	Quadrupolar Mode: 0.12	*X*-axis: [−40,40] *Y*-axis: [−40,40]				
[16]	Unipolar Mode: 0.07	*X*-axis: [−100,150] *Y*-axis: [−150,150]	Medium (Three Decoupled Unipolar Coils, 390×400 mm)	Medium (Three-Inverter Control)	Unipolar and Bipolar	–
	Bipolar Mode: 0.10	*X*-axis: [−50,200] *Y*-axis: [−50,50]				
[17]	Unipolar Mode: 0.30	*X*-axis: [−150,150]	High (Multiple Self-Decoupled Coils, 300×300 mm)	High (Real-time Vector Synthesis)	Unipolar, Bipolar and Quadrupolar	Reverse Winding
	Bipolar Mode: 0.22	*X*-axis: [−150,150] *Y*-axis: [−60,60]				
	Quadrupolar Mode: 0.07	*Y*-axis: [−60,60]				
Proposed	**Unipolar Mode: 0.14**	***X*-axis: [−120,120]** ***Y*-axis: [−150,150]**	**Low (Two Decoupled Unipolar Coils, 300×300 mm)**	**Low (Single Inverter)**	**Unipolar and Bipolar**	**Reverse Winding**
	Bipolar Mode: 0.14	***X*-axis: [−150,150]** ***Y*-axis: [−60,60]**				

The bold values are used to indicate the parameters of the system proposed.

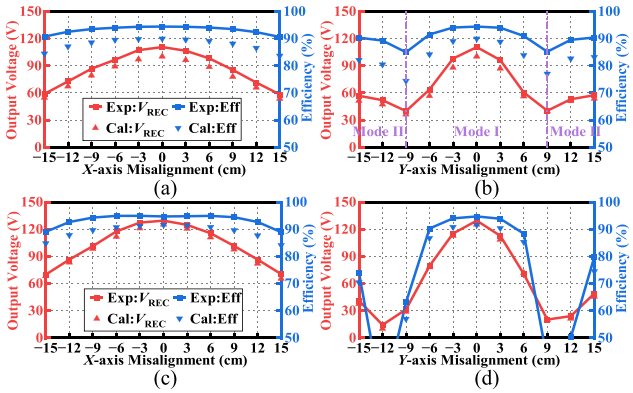

Fig. 11. Output voltage and efficiency in Mode II. (a) Proposed (*X*-axis). (b) Proposed (*Y*-axis). (c) Traditional (*X*-axis). (d) Traditional (*Y*-axis).

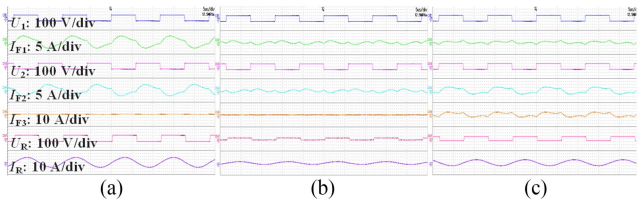

Fig. 12. Waveforms in Mode I. (a) Perfectly aligned. (b) Maximum *X*-axis misalignment. (c) Maximum *Y*-axis misalignment.

traditional systems. However, as misalignment increases, traditional system efficiency declines sharply. The proposed system addresses this by switching modes when the output voltage reaches a threshold, altering the transmitting current direction to enhance coupling and maintain efficiency. This approach ensures interoperability and superior misalignment tolerance compared to traditional systems.

The system waveforms are shown in Figs. 12 and 13. The waveforms show that the current is negative during the voltage rise edge, and the current phase lags behind the voltage, proving

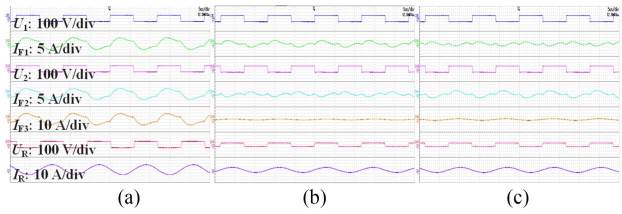

Fig. 13. Waveforms in Mode II. (a) Perfectly aligned. (b) Maximum *X*-axis misalignment. (c) Maximum *Y*-axis misalignment.

that the system achieves zero voltage switch (ZVS) and operates in a resonant state. The proposed topology maintains ZVS across the entire misalignment range, effectively reducing switching losses.

A summary of existing and proposed solutions is presented in Table II. The proposed system demonstrates superior performance across multiple metrics. In terms of power density, the proposed system achieves 0.14 W/cm^3 in both modes, exceeding most existing schemes. For system efficiency exceeding 80%, the effective misalignment range is −90 to 90 mm along the *X*-axis and −150 to 150 mm along the *Y*-axis for the unipolar receiving coil, and −150 to 150 mm on the *X*-axis and −60 to 60 mm on the *Y*-axis for the bipolar receiving coil. This result confirms that the proposed system maintains efficient energy transfer even under large misalignment conditions.

Besides, the proposed system features low coil complexity and control complexity. The proposed coil configuration employs only two decoupled unipolar coils, offering a simple and efficient structure; the control system requires only a single inverter, significantly reducing volume and cost. Furthermore, the system is compatible with both unipolar and bipolar coil, achieving a balance of efficiency and simplicity in both structure and control strategy.

In conclusion, the proposed system minimizes both coil and control complexity, while still achieving high power density and a broad efficiency range. These attributes make it particularly

well suited for applications that demand high system integration and simplified control.

V. Conclusion

This letter proposes a WPT system for EVs based on two decoupled unipolar transmitting coils. The proposed novel decoupling method enables power transmission to different types of receiving coils. The transmitting side employs a dual LCC topology, adjusting the transmitting current direction in by altering the conduction sequence of the inverter to accommodate both unipolar and bipolar receiving coils. Experimental results validate the interoperability of the proposed wireless charging system. Additionally, an innovative mode-switching control strategy maintains high-efficiency output under misalignment conditions. Compared to existing solutions, the proposed system offers higher power density and efficiency, providing a promising solution for applications requiring high system integration and simplified control.

References

[1] Z. Yan et al., "Free-rotation wireless power transfer system based on composite anti-misalignment method for auvs," *IEEE Trans. Power Electron.*, vol. 4, no. 38, pp. 4262–4266, Apr. 2023.

[2] C. Cai, J. Wang, H. Nie, P. Zhang, and Z. Lin, and Y.-G. Zhou, "Effective-configuration WPT systems for drones charging area extension featuring quasi-uniform magnetic coupling," *IEEE Trans. Transp. Electrif.*, vol. 3, no. 6, pp. 920–934, Sep. 2020.

[3] R. Xie, Y. Chen, Z. Huang, X. Chen, and X. Mao, and Y. Zhang, "A series of dual-frequency hybrid topologies with vertical and horizontal misalignment tolerance performance in inductive power transfer systems," *IEEE Trans. Transp. Electrif.*, vol. 4, no. 11, pp. 10203–10211, Aug. 2025.

[4] Y. Zhang et al., "A lightweight bidirectional wireless energy carrier without drone-side compensation and ferrite for devices in inaccessible places," *IEEE Trans. Ind. Electron.*, to be published, doi: 10.1109/TIE.2025.3581191.

[5] D. Kraus, G. A. Covic, H. Herzog, P. A. J. Lawton, and F. J. Lin, "Design and assessment of an interoperable wireless power transfer system using an impedance-based method," *IEEE Trans. Power Electron.*, vol. 2, no. 38, pp. 2768–2781, Feb. 2023.

[6] A. Munsi, S. Pradhan, and K. Aditya, "Advancements in inductive wireless power transfer: A comprehensive review," *Chin. J. Elect. Eng.*, to be published, doi: 10.23919/CJEE.2025.000136.

[7] M. Abdelraziq and Z. Pantic, "Design and optimization of a reconfigurable powertrain-integrated IPT receiver for UAS wireless charging," *IEEE J. Emerg. Sel. Top. Power Electron.*, to be published, doi: 10.1109/JESTPE.2025.3576932.

[8] H. Wang and K. W. E. Cheng, "Analysis, design, and validation of a decoupled double-receiver wireless power transfer system with constant voltage outputs for industrial power supplies," *IEEE Trans. Ind. Inform.*, vol. 1, no. 19, pp. 362–370, Jan. 2023.

[9] X. Liu, X. Li, Z. Liu, Q. Zhang, and S. Li, "Interoperability analysis and improvement of wireless charging system for electric vehicle application with different compensation networks," in *Proc. IEEE 3rd Int. Elect. Energy Conf.*, 2019, pp. 839–844.

[10] A. Bilal, G. Covic, and S. Kim, "Interoperability of magnetic pads with intermediate coils and different primaries," in *Proc. Wireless Power Week*, 2022, pp. 497–502.

[11] A. Ahmad, M. S. Alam, and A. A. S. Mohamed, "Design and interoperability analysis of quadruple pad structure for electric vehicle wireless charging application," *IEEE Trans. Transp. Electrif.*, vol. 4, no. 5, pp. 934–945, Dec. 2019.

[12] W. Pan, C. Liu, H. Tang, Y. Zhuang, and Y. Zhang, "An interoperable electric vehicle wireless charging system based on mutually spliced double-d coil," *IEEE Trans. Power Electron.*, vol. 3, no. 39, pp. 3864–3872, Mar. 2024.

[13] G. Yang et al., "Interoperability improvement for rectangular pad and DD pad of wireless electric vehicle charging system based on adaptive position adjustment," *IEEE Trans. Ind. Appl.*, vol. 3, no. 57, pp. 2613–2624, May/Jun. 2021.

[14] Y. Li, X. Chu, Z. Li, Y. Zhai, and H. Qin, "A vertical overlapping decoupled coil for wireless power transfer with high interoperability," *IEEE Trans. Power Electron.*, vol. 10, no. 40, pp. 16032–16041, Oct. 2025.

[15] A. Zaheer, H. Hao, G. A. Covic, and D. Kacprzak, "Investigation of multiple decoupled coil primary pad topologies in lumped IPT systems for interoperable electric vehicle charging," *IEEE Trans. Power Electron.*, vol. 4, no. 30, pp. 1937–1955, Apr. 2015.

[16] Y. Zhang et al., "Interoperability study of electric vehicle wireless charging system based on three decoupled nonoverlapping unipolar transmitting coils," *IEEE Trans. Transp. Electrif.*, vol. 4, no. 10, pp. 8630–8639, Dec. 2024.

[17] Y. Zhang, Z. Huang, Z. Shen, R. Xie, and X. Chen, and X. Mao, "Interoperability and misalignment tolerance of electric vehicle wireless charging system based on multiple self-decoupled transmitting coils and vector synthesis strategy," *IEEE Trans. Power Electron.*, vol. 40, no. 5, pp. 7512–7522, May 2025.